Optimal Surface Profile Design of Deployable Mesh Reflectors via a Force Density Strategy

Dongwu YANG [1,2,3*], Jingsheng LIU [3], Yiqun ZHANG [1,2] and Shuxin ZHANG [1,2]
1 School of Electromechanical Engineering, Xidian University, Xi'an, China 710071
2 Key Laboratory of Electronic Equipment Structure Design, Ministry of Education, Xi'an, China 710071
3 School of Engineering, University of Hull, Hull, UK, HU6 7RX

***Abstract*—Based on a force density method coupled with optimal design of node positions, a novel approach for optimal surface profile design of mesh reflectors is presented. Uniform tension is achieved by iterations on seeking optimum coefficients of the force density. The positions of net nodes are recalculated in each iteration so that the faceting rms error of the reflector surface is minimized. Applications of both prime focus and offset configurations are demonstrated. The simulation results show the effectiveness of the proposed approach.**

***Index Terms*—Antenna surface design, Deployable mesh reflectors, Cable net, Uniform tension, Force density method**

1. Introduction

The technological development of modern space-borne deployable antennas is trending toward both larger apertures and greater accuracy [1, 2]. Large deployable mesh reflectors like the AstroMesh [3] have brought continuous interest in research and development in the past several decades.

As illustrated in Fig.1, the AstroMesh reflector is based on a tension truss concept. The outer supporting ring truss, called deployable rim truss, is connected to a cable net structure and has sufficient stiffness and high stability to support the cable-net structure once deployed. The cable net structure is comprised of two identical paraboloid-shaped nets (i.e., a front net and a rear net) and a series of vertical tension ties. The tension-tie assembly imposes vertical tensile forces between the front net and the rear net to pretension the cable-net structure. The radio frequency (RF) reflective mesh is attached to the backside of the front net and is pretensioned fairly isotropically and uniformly. The deployed reflector is approximately formed by flat triangular facets of the RF reflective mesh and the vertices of the mesh facets are nodes of the front net. Namely, the reflective mesh is shaped by the front net.

For concentrating radio frequency radiation, the operating reflective mesh needs to maintain an exact paraboloidal shape. Proper design of the cable-net structure to minimize the faceting rms error and to optimize the error distribution of the mesh surface is essentially important to the performance of such space structures [2]. Meanwhile, uniform tension in the supporting cable net is desirable from geometrical and mechanical point of view. It is the most stable position since it corresponds to the minimum potential energy configuration [4].

Until recently, several design methods have been published on antenna cable net configuration designs. Tibert [5] presented a shape-optimal design approach for searching minimal length mesh configurations with three shape-forming steps. Morterolle et al. [4] proposed a numerical form-finding approach for calculating the geodesic paraboloidal mesh configurations using the force density method (FDM). Li et al. [6, 7, 8] proposed design methods to generate geodesic cable nets for mesh reflector, a pretension design method based on the projection principle for mesh reflector and a pretension design method considering multi-uncertainty. Shi et al. [9, 10] proposed design methodologies to automatically generate pseudogeodesic mesh geometries of spherical and parabolic reflector surfaces. Additionally, when considering the elastic deformation of rim trusses, several techniques have been introduced to compensate the deformation of the supporting trusses [11, 12, 13] after form-finding for the cable net configurations.

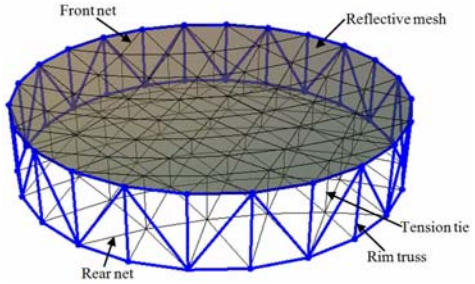

Fig.1 AstroMesh reflector and its components

Among all these researches, only the approach proposed by Morterolle et al. [4] guarantees a uniform tension in the cable-net within the reflective zone. But their approach has one common imperfect feature with all the others: the cable net nodes designed are always exactly on a paraboloidal surface. According to our previous work [14], if and only if all the projections of triangular facets fall exactly into equilateral triangles on the aperture plane, the cable net nodes designed could be exactly on an appointed paraboloidal surface to minimize the axial faceting rms error within the hexagonal reflective zone. Otherwise, it might not be the best idea putting all the cable net nodes exactly on a paraboloidal surface.

In this paper, it is attempted to get better results in the far field patterns of concerned reflectors by integrating a procedure on optimizing the positions of the cable net nodes with the numerical form-finding procedure proposed by Morterolle et al.

[1] Associate Professor, Research Institute on Mechatronics, ydw_1978@126.com.

[4].

This paper is organized as follows. Section 2 presents the coordinate systems used when describing the revised form-finding approach proposed by us. In section 3, systematic faceting errors of mesh reflectors and the method to minimize the faceting errors are investigated. Section 4 presents the form-finding approaches proposed by both Morterolle et al. [4] and ourselves with emphasis on the differences. In section 5, two applications, for a prime focus and an offset paraboloidal reflector, are shown to illustrate the efficiency of the method. Section 6 gives a brief conclusion of this paper.

2. Coordinate systems

Generally, the reflector surface of a paraboloidal antenna is defined by the intersection of a parent rotary paraboloid (with diameter D_p) and a cylinder (diameter D_a) parallel to the paraboloid axis which characterizes the antenna aperture. The paraboloidal antennas are based on the same principle: all incident rays parallel to the paraboloid axis converge to the focal point (feed) after reflection on the surface. Conversely, all emitted rays are reflected out parallel to the paraboloid axis.

For a "prime focus" antenna (Fig.2), the axes of the parent paraboloid and the cylinder are coincident. The reflector surface is thus a paraboloid of revolution ($D_p = D_a$)。 For a Cartesian coordinate system ($\vec{X},\vec{Y},\vec{Z}$), $\vec{Z}$ being the axis of revolution, the equation describing this axi-symmetric parabolic surface is

$$Z = (X^2 + Y^2)/(4F) \tag{1}$$

where F is the focal length.

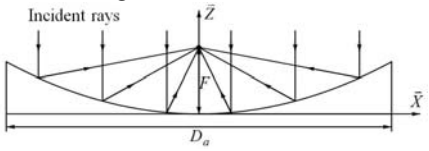

Fig.2 Prime focus paraboloidal reflector

One drawback of the axi-symmetric reflector is that the feed and its support are bulky and can block a part of the rays. To eliminate this problem and improve performance, antennas with offset feed are used. The cylinder axis is therefore separated to the paraboloid rotary axis with an offset distance d and $D_p = 2d + D_a$ (Fig. 3). It can be proven that the rim of the resulted reflector surface is a flat ellipse. The coordinate system ($\vec{X},\vec{Y},\vec{Z}$) is usually named as "global coordinate system", and the coordinate system ($\vec{X}',\vec{Y}',\vec{Z}'$) is named as "local coordinate system" which has its origin on the surface center O′ and with an angle φ ($\tan\varphi = d/(2F)$) between the $\vec{X}'$ axis and the plane perpendicular to the paraboloid axis.

For a mesh reflector structure like the AstroMesh[3], the tension ties are usually parallel to the $\vec{Z}'$ axis. The equilibrium equations of the nodes used in the force density method (FDM) are usually set up in the local coordinate system ($\vec{X}',\vec{Y}',\vec{Z}'$). Since it is more convenient to find optimal positions of cable net nodes in the global coordinate system, transformations have to be performed between the two coordinate systems in our form- finding approach.

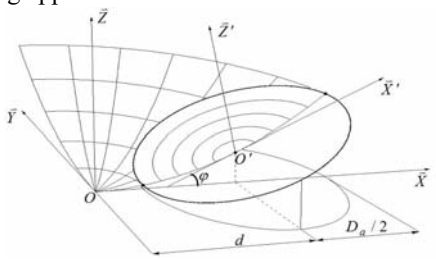

Fig.3 Axonometric view of offset paraboloidal surface

Given an arbitrary point P, which is described in the global coordinate system as $(X,Y,Z)^{\mathrm{T}}$ and in the local coordinate system as $(X',Y',Z')^{\mathrm{T}}$, the relationship between the two coordinate systems of the point P can be defined as

$$\begin{pmatrix} X \\ Y \\ Z \end{pmatrix} = \mathbf{T}\begin{pmatrix} X' \\ Y' \\ Z' \end{pmatrix} + \begin{pmatrix} X_{O'} \\ Y_{O'} \\ Z_{O'} \end{pmatrix} \tag{2}$$

or

$$\begin{pmatrix} X' \\ Y' \\ Z' \end{pmatrix} = \mathbf{T}^{-1}\left(\begin{pmatrix} X \\ Y \\ Z \end{pmatrix} - \begin{pmatrix} X_{O'} \\ Y_{O'} \\ Z_{O'} \end{pmatrix}\right) \tag{3}$$

where $(X_{O'},Y_{O'},Z_{O'})^{\mathrm{T}} = (d,0,d^2/(4F))^{\mathrm{T}}$ is the origin of the local coordinate system described in the global coordinate system.

For a prime focus antenna, such a local coordinate system is indeed not required but is assumed to exist and coincide with the global coordinate system. In this case, the transformation matrix should be an identity matrix and $(X_{O'},Y_{O'},Z_{O'})^{\mathrm{T}}$ have zero values.

3. Position optimization of cable net nodes

3.1 Reflector surface error

The ideal mathematical shape defined by Eq. (1) is however purely theoretical since it has to be realized by a faceted mesh stretched on the tension truss (cable net structure). The topology of the cable net determines the forms and dimensions of the flat facets. The deviations of the faceted paraboloidal reflector from its ideal shape cause, in general, loss of gain and pattern degradation.

The effects of surface deviations on the radiation pattern and gain may be predicated from the actual distribution of surface deviations over the aperture. A simple approximate method for computing these effects is presented by Ruze [15], as the following well-accepted form for the gain:

$$\mathrm{G} = G_0 e^{-\delta_0^2} \tag{4}$$

$$\delta_0^2 = \frac{\int_A \delta(\vec{r})^2 f(\vec{r}) dS}{\int_A f(\vec{r}) dS} \tag{5}$$

where G and G_0 are the gains of antenna with and without

errors respectively; $\vec{r}$ is an aperture position vector; the function $\delta(\vec{r})$ represents effective surface deviation from the best-fit paraboloid for deterministic errors; $f(\vec{r})$ is the aperture illumination function; A represents the aperture area of the antenna reflector; δ_0^2 is the mean square of the effective surface deviations and $\delta_0 = \sqrt{\delta_0^2}$ is the surface rms error. The effective surface deviation is defined as one half of the change in the RF path length. The best-fit paraboloid is a chosen paraboloid so that an imperfect surface can be best approximated by, or in another word, expression (5) falls in a minimum value.

The relation between an axial deviation $\Delta z(\vec{r})$ and the corresponding effective surface deviation is

$$\delta(\vec{r}) = \frac{\Delta z(\vec{r})}{1+(X^2+Y^2)/(4F^2)} \tag{6}$$

Then (5) may be rewritten as follows,

$$\delta_0^2 = e_s / c \text{ or } \delta_0 = \sqrt{e_s / c} \tag{7}$$

where,

$$c = \int_A f(\vec{r}) dS \tag{8}$$

$$e_s = \int_A \Delta z^2(\vec{r}) w(\vec{r}) dS \tag{9}$$

$$w(\vec{r}) = \frac{f(\vec{r})}{(1+(X^2+Y^2)/(4F^2))^2} \tag{10}$$

The surface error investigated in this paper is only that caused by approximating an ideal paraboloid surface with mesh facets. e_s will be named as the faceting square error and δ_0 as the faceting rms error in the following sections.

3.2 Aperture illumination function

The aperture illumination function $f(\vec{r})$ is equivalent, but not identical, to the radiation pattern of the feed in the focal point. This function determines the illumination efficiency of the antenna, which is the ratio of the gain of the antenna to that of a uniformly illuminated aperture. The illumination function is normally characterized by the "edge taper", i.e. the level of the illumination at the edge of the reflector compared to that in the center. However, different functional forms of the illumination function with the same edge level can result in different values for the illumination efficiency.

An aperture illumination (field distribution) function with circularly symmetric amplitude and constant phase front is used here, which is the parabolic to a power n on a pedestal distribution and has the form of

$$f(\vec{r}) = \tau + (1-\tau)(1-(2|\vec{r}|/D_a)^2)^n \tag{11}$$

where τ represents the edge level while the level in the aperture center is normalized to one, and n represents the aperture taper. Both of these two parameters must be chosen properly to approximating the aperture field from an ideal reflector surface.

3.3 Node position optimization

From Eq. (4) to (10), it is clear that for an optimal surface profile design of a mesh reflector, the faceting square error e_s should be as small as possible to get a higher gain.

Let us start with a more detailed expression of e_s with design variables involved. For the front net of a mesh reflector where the $\vec{X}$ and $\vec{Y}$ coordinates of all the nodes are given, the nodes are considered to be movable along the $\vec{Z}$ direction.

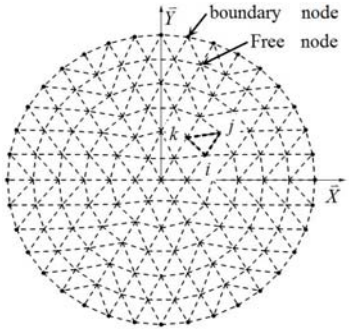

Fig. 4 Cable net projection on antenna aperture

Considering a (flat) triangular facet isolated from the cable net, with i, j and k as its vertexes (the projection on antenna aperture is shown in Fig.4), the space plane determined by the facet can be denoted as a function of the vertexes coordinates in $\vec{Z}$ direction as follows,

$$Z = B_i(\vec{r})Z_i + B_j(\vec{r})Z_j + B_k(\vec{r})Z_k \tag{12}$$

$$B_i(\vec{r}) = \frac{(Y_k - Y_j)X + (X_j - X_k)Y + (X_k Y_j - X_j Y_k)}{X_i Y_k - X_i Y_j + X_j Y_i - X_j Y_k + X_k Y_j - X_k Y_i}$$

$$B_j(\vec{r}) = \frac{(Y_k - Y_i)X + (X_i - X_k)Y + (X_k Y_i - X_i Y_k)}{X_i Y_j - X_i Y_k + X_j Y_k - X_j Y_i + X_k Y_i - X_k Y_j}$$

$$B_k(\vec{r}) = \frac{(Y_j - Y_i)X + (X_i - X_j)Y + (X_j Y_i - X_i Y_j)}{X_i Y_k - X_i Y_j + X_j Y_i - X_j Y_k + X_k Y_j - X_k Y_i}$$

where $B_i(\vec{r})$, $B_j(\vec{r})$ and $B_k(\vec{r})$ are linear functions of X and Y, and (X_m, Y_m, Z_m) $(m = i, j, k)$ are the coordinates of the vertex points.

The faceting square error of the triangular facet can be written in a more detailed form as,

$$e_s^{ijk} = \int_{A_{ijk}} (B_i(\vec{r})Z_i + B_j(\vec{r})Z_j + B_k(\vec{r})Z_k - (X^2+Y^2)/(4F))^2 w(\vec{r}) dS \tag{13}$$

where A_{ijk} represents the projection area of the triangular facet on the antenna aperture.

From Eqs. (12) and (13) it can be seen that e_s^{ijk} should be a pluralistic quadratic function of Z_i, Z_j and Z_k. Also, it can be noticed that an accurate integral of Eq. (13) might not be easy because of the complicated form of $w(\vec{r})$ (Eqs. (10) and (11)). However, the result of Eq. (13) can be obtained by numerical integral methods with suitable accuracy. In this paper, the quadrature rule of order 6 with 12 integral points given by Dunavant [16] is used. Although quadrature rules of higher degree can be used, it does not make significant difference.

The faceting square error e_s for the whole reflector, which is a summation of faceting square errors for all facets in the cable net, can be expressed in a pluralistic quadratic function of the $\vec{Z}$ direction coordinates of the net nodes, and its minimum value can be easily figured out. Meanwhile, the node positions, that make the e_s reaching its minimum value, determine a cable net with an optimal surface profile.

Moreover, since all the boundary nodes of a cable net generally need to be on a plane from structural point of view (the loops of a deployed rim truss should be flat), all the $\vec{Z}'$ direction coordinates of boundary nodes should have a same value. This makes it difficult to minimize the faceting square error e_s, since the expression of error e_s in Eq. (9) is for the global coordinate system. Fortunately, an offset of the paraboloid has the same effects with an offset of boundary nodes as a whole in the $\vec{Z}$ direction, and the ideal reflector rim implies a flat spatial circle or ellipse when the antenna aperture is a circular one. So the following Eq. (14) are preferably used instead of Eq. (13) when the faceting square error e_s is calculated. Also, the boundary nodes of the cable net are fixed on the ideal paraboloidal surface during the procedure of node position optimization.

$$e_s^{ijk} = \int_{A_{ijk}} (B_i(\vec{r})Z_i + B_j(\vec{r})Z_j + B_k(\vec{r})Z_k - (X^2+Y^2)/(4F) - t)^2 w(\vec{r})dS \quad (14)$$

where t represents an offset distance of paraboloid in $\vec{Z}$ direction. Accordingly, the best-fit paraboloid for the resulted reflector is defined by

$$Z = (X^2+Y^2)/(4F) + t \quad (15)$$

Incidentally, when a best-fit paraboloid surface needs to be found for a given net without variation of the focal length, Eqs.(14) and (15) can also be used for determining the best-fit paraboloid and thus for calculating the faceting square error e_s or the surface rms error δ_0.

4. Form-finding strategies based on FDM

4.1 Basis of the force density method (FDM)

The principle of FDM is to linearize the equilibrium equations of the nodes connecting the tensile cable elements. Considering an isolate node i which is connected to c_i cables of length l_j with tension T_j ($j = 1,2,\cdots,c_i$) and without external forces (Fig. 5), the node equilibrium, written in the $\vec{X}'$ direction of a coordinate system ($\vec{X}',\vec{Y}',\vec{Z}'$), implies that

$$\sum_{j=1}^{c_i} T_j(X'_j - X'_i)/l_j = 0 \quad (16)$$

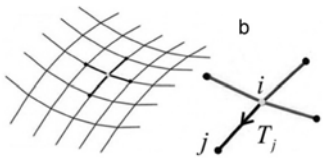

Fig.5 Cable net equilibrium (from Morterolle [4])

The same relations may also be written in the $\vec{Y}'$ and $\vec{Z}'$ directions. There is no need to set up such relations for the boundary nodes which define the anchoring conditions and have no degree of freedom.

Then, a "force density" coefficient q_j for every cable element is introduced to linearize these nonlinear equilibrium equations by defining

$$q_j = T_u / l_j \quad (17)$$

where T_u is a required uniform tension. It results in the following expression:

$$\sum_{j=1}^{c_i} q_j(X'_j - X'_i) = 0 \text{ and thus } X'_i = (\sum_{j=1}^{c_i} q_j X'_j)/(\sum_{j=1}^{c_i} q_j) \quad (18)$$

Once these linear equations are solved, the global equilibrium and new positions for all the free nodes, corresponding to the given coefficient q_j , are obtained. Cable tensions are then evaluated by $T_j = q_j l_j$.

The principle of the FDM strategy is to evaluate the force density coefficients iteratively and eventually obtain the required uniform tension T_u . For instance, if step p gives tension T_j^p and length l_j^p for an element j , the new coefficient used in the following step is

$$q_j^{p+1} = T_u / l_j^p \quad (19)$$

If the boundary conditions make it possible to form a uniformly tensioned cable net, this method generally converges to a solution. However, conditions for a guaranteed convergence are still under investigation, and this analysis is indeed difficult to achieve since it depends on many factors such as the net topology and the anchoring conditions.

4.2 Form-finding strategy proposed by Morterolle

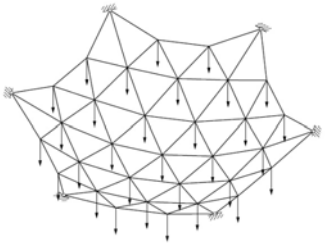

Fig.6 Cable net formed by out-of-plane loads (from Tibert [5])

To make a cable net of mesh reflector and form a parabolic surface, the tension ties, which connect the front and rear cable nets, provide the cable nets with additional forces in $\vec{Z}'$ direction (Fig.6). The force values of the tension ties are chosen to ensure the proper nodes positioning.

In the method proposed by Morterolle, all nodes of cable net were forced exactly positioning on a paraboloid surface. From an initial net and a given set of force density coefficients q_j , the equilibrium position of a node i in $\vec{X}'$ and $\vec{Y}'$ directions was determined by the FDM (Eq. (18)). With these two coordinates

and the surface equation described in the coordinate system ($\vec{X}', \vec{Y}', \vec{Z}'$), the corresponding accurate position along $\vec{Z}'$ was determined. For a prime focus configuration, the surface equation had the same form as Eq. (1), but it would be different from Eq. (1) for an offset configuration (the details can be found in Ref. [4]). Lengths and tensions in the cable elements were then calculated and the condition of uniform tension was tested. The process was resumed by iteratively changing the force density coefficients (Eq. (17)) until (i) a uniform tension T_u was obtained in all the cables, and (ii) the node positions did not vary (stable at equilibrium positions).

If the process converges, a uniformly tensioned synclastic cable net with every node exactly on the parabolic surface was obtained. The necessary force in the tension tie to equilibrate the node i along $\vec{Z}'$ direction could be calculated by

$$F_{Z_i'} = \sum_{j=1}^{c_i} q_j (Z_j' - Z_i') \tag{20}$$

The criteria used for convergence were the followings. To satisfy the uniform tension requirement, the difference with the objective T_u must be lower than a tolerance tol_T (set to 0.1%). Moreover, a node was considered stable in position if, between two consecutive iterations, the norm of its coordinate variations $\Delta\vec{X}_i'$ was inferior than tol_X (set to 10^{-6} m). There was another criterion to check about the equilibrium of the nodes in Ref. [4], but we consider it as a convergence criterion for the results of linear force density equations and therefore do not list it here.

4.3 Our form-finding strategy

The procedure of form-finding proposed in this paper is similar but different from the one given by Morterolle [4]. In our method, when the corresponding position along $\vec{Z}'$ is calculated, after the equilibrium position of a node i in $\vec{X}'$ and $\vec{Y}'$ directions is obtained by the FDM (Eq. (18)), the node i will not position exactly on the objective paraboloidal surface any more. Instead, an optimal position for node i is sought by using the approach detailed in section 3. For instance, if step p gives an equilibrium position for node i ($X_i'^p$ and $Y_i'^p$), the coordinates $(X_i'^p, Y_i'^p, Z_i'^{p-1})$ of node i are firstly transformed to the global coordinate system ($\vec{X}, \vec{Y}, \vec{Z}$) based on Eq. (2). Here, $Z_i'^{p-1}$ is the $\vec{Z}'$ direction coordinate of node i last updated. Then, after the new position of node i is obtained by the optimization procedure described in Section 3, Eq. (3) is used to transform the coordinates of node i back to the coordinate system ($\vec{X}', \vec{Y}', \vec{Z}'$). It should be mentioned that, the coordinates $X_i'^p$ and $Y_i'^p$ will also be slightly changed when $Z_i'^p$ is finally figured out, but these small changes have no significant influence on the characteristics of convergence of the form-finding process. The overall method is presented in Fig.7 as an algorithm.

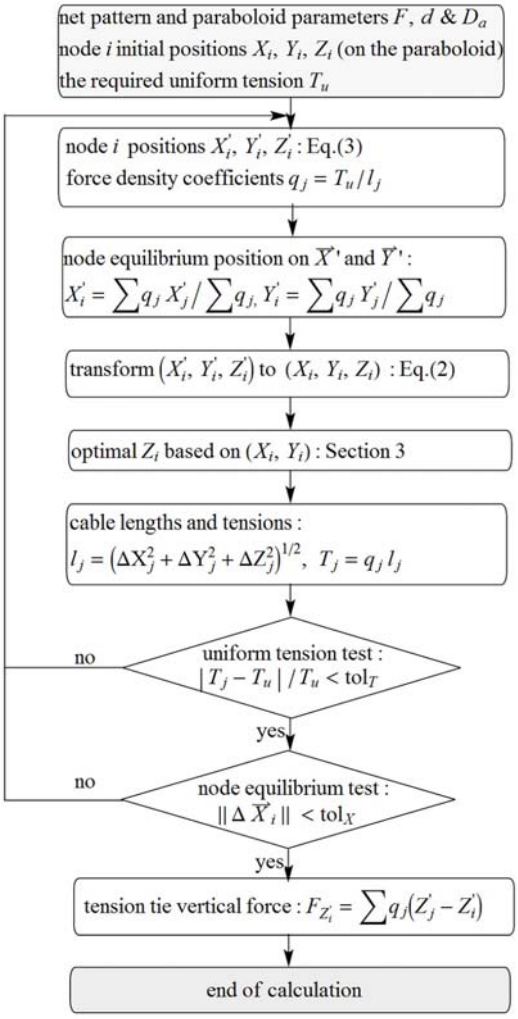

Fig.7 Algorithm for geometry construction

Compared to the method proposed by Morterolle [4], this approach takes a little more time because of more calculations involved in calculating and minimizing of the faceting square error. Therefore it may be advisable to use the node positions resulted by Morterolle's method as the initial node positions just for saving time. In order to verify the feasibility of our form-finding strategy as a whole, the initial net patterns and node positions used here are the same as the ones Morterolle used, which are generated as follows. Generally, the initial net pattern for a paraboloid mesh reflector is located inside a circle with a diameter of D_a on the antenna aperture plane (an example of the initial net pattern is shown in Fig. 4). The circle has its center at $X = 0$ and $Y = 0$ for a prime focus configuration, or at $X = d$ and $Y = 0$ for an offset configuration. Then, the $\vec{Z}$ direction coordinates are figured out by the relationship in Eq. (1). This means that all nodes of the cable net have their initial positions exactly on the paraboloid surface, and the boundary nodes, which are located on the reflector rim truss, are all fixed points in the whole procedure of the form-finding.

5. Applications

The method has been applied to several applications. Here, only two of them are illustrated and both are originated from Ref [4]. The first one has a prime focus configuration, and the second has an offset configuration. Both of the paraboloidal reflectors have a circular aperture (viewed from the boresight direction) with a diameter of $D_a = 12$ m. The focal ratios (defined as F/D_p) are 0.4 and 0.45 respectively, and the offset distance d for the latter is 8.3m.

In order to make a comparison of the resulting nets obtained by the approaches proposed in Ref. [4] and by us, the far field radiation patterns of the corresponding mesh reflector systems were calculated and used as the evaluation basis for the resulting nets. All the electromagnetic calculations concerned were carried out using the GRASP (version 9.7) software.

It is started from calculating the radiation patterns of a reflector system with an ideal reflector surface, which has the same parameters of the mesh reflector concerned. The reflector is illuminated by a corrugated horn with its aperture at the focal point of the reflector and pointed towards the centre of the reflector. The corrugated horn radiates a Gaussian beam providing an edge illumination of -12 dB. The feed is linearly polarised in the plane which contains the axes of both $\vec{X}$ and $\vec{Z}$. The working (or operating) frequency was determined based on a pre-estimate of the faceting rms error of the resulting mesh reflector which was approximately 5mm for the prime focus case or 0.5mm for the offset case. Thus, the single-reflector systems were analyzed at 2 GHz for the prime focus case and at 20GHz for the offset case. Based on the resulting near field patterns for the ideal reflector surfaces, the parameters τ and n were chosen properly for the aperture illumination functions, which were $\tau = 0.199526, n = 2.35$ for the prime focused case, and $\tau = 0.251189, n = 1.80$ for the offset.

For convenience, the resulting cable net and the corresponding mesh reflector resulted from Ref. [4] are both denoted by mesh0, and the ones resulted from this paper aiming at minimizing the faceting square error e_s are both denoted by mesh1.

Moreover, it would be easier for structural people to measure the surface rms error of a reflector if the function $w(\vec{r})$ described in Eq. (10) takes a constant unit value. It is interesting to have an investigation of such a case. That is to say, the faceting square error is replaced by the axial faceting square error which is defined by

$$e_{zs} = \int_A \Delta z^2(\vec{r})\, dS \qquad (21)$$

The resulting cable net and the corresponding mesh reflector resulted from minimizing the axial faceting square error are both denoted by mesh2.

It should be mentioned that, if Eq. (21) is used the faceting square error or rms error should be calculated by

$$\delta_0^2 = e_{zs}/\tilde{c} \quad \text{or} \quad \delta_0 = \sqrt{e_{zs}/\tilde{c}} \qquad (22)$$

instead of Eq. (7), where $\tilde{c}$ is the area of antenna aperture.

5.1 Prime focus configuration

5.1.1 Calculation of the nets

In the prime focus case, a 6 by 6 diamatic net pattern is investigated. The initial net pattern is composed of 6 disc sectors where each boundary side is divided into 6 elements. The initial net pattern on the antenna aperture is shown in Fig. 4. The $\vec{Z}$ coordinates of all the initial nodes are figured out by the relationship in Eq. (1).

For a 100N uniform tension in the net, the form-finding method converged no matter which objective function (e_s or e_{zs}) was used in optimizing the node positions. Because the differences between the resulting mesh1 and the others are too small to distinguish in a figure, only the resulting mesh1 is shown in Fig.8. Other details of the results are listed in Table 1 for a comparison.

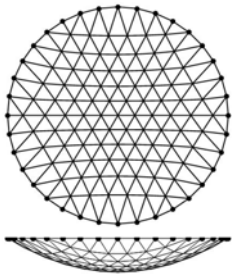

Fig.8 Symmetric 6 by 6 diamatic net under uniform tension

Table 1 Form-finding result for the prime focus configuration

	Mesh0	Mesh1	Mesh2
Iterations	67	64	65
converged max$\lvert(T_j - T_u)/T_u\rvert$	3×10^{-7}	7×10^{-7}	8×10^{-7}
converged max$\lVert\Delta\vec{X}_i\rVert$ (mm)	0.00096	0.00084	0.00098
Faceting rms error(mm)	5.62	4.13	4.19
Parameter t (mm)	14.79	26.84	25.05
Average force in tension ties (N)	32.17	31.79	31.90
Standard deviation of forces in tension ties (N)	2.60	3.21	3.71

From Table 1, it can be seen that the uniform tension requirement is always well satisfied when the nodes converge to their stabilized equilibrium positions. The faceting rms errors of the mesh1 and mesh2 are close and both of them are better than that of the mesh0. Even though there are some differences in the standard deviations of forces in the tension ties, the differences in the average forces are no significant.

It should be mentioned that all the faceting rms errors showed in this table were figured out according to Eq. (7), even though a different equation (Eq. (22)) was used to obtain the configuration of the mesh2. The focus position (corresponding to the parameter t in Eq. (14)) of the best-fit paraboloid for the mesh2 was determined by minimizing the faceting rms error in Eq. (22). These resulted parameters are 25.11 mm for t and 6.14 mm for the resulted faceting rms error.

It should also be mentioned that the number of iteration steps counted here is smaller than that reported in Ref. [4]. It was approximately 200 iterations for convergence to mesh0. The reason for the difference is that the number of iterations for solving the force density equations (Eq. (18)) was not counted in.

5.1.2 Radiation patterns

Even if there are other error sources in a real mesh reflector such as manufacturing, mesh saddling, and thermal extremes. It is assumed here that the RF reflective mesh will exactly follow the shape of the cable net and there is no other but faceting error in the resulted mesh reflector. Also, the wave leakage through the mesh is ignored.

The co-polar far-field radiation patterns, calculated at 2 GHz by the physical optics (PO) method in both the E-plane and the H-plane, are shown in Fig.9 and Fig.10, respectively. Where, both the mesh1 and mesh2 give radiation patterns closer to the one for the ideal surface than the mesh0 does, and the radiation pattern for the mesh1 is not significantly better than the one for the mesh2, even though the mesh2 was obtained aimed at minimizing the axial faceting square error e_{zs}, which has a much simpler form than the faceting square error e_s.

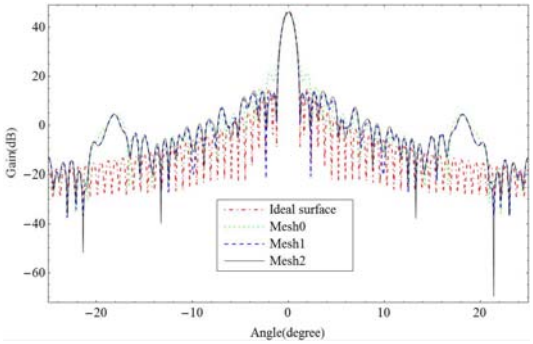

Fig.9 Far field patterns in E-Plane for prime focus case

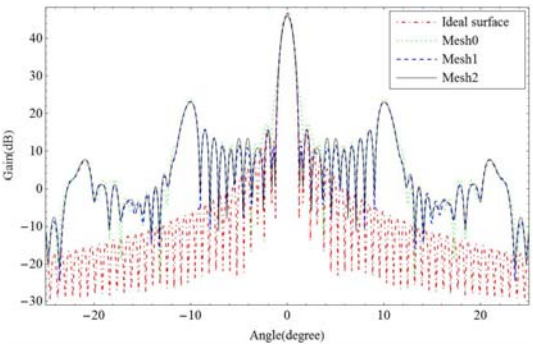

Fig.10 Far field patterns in H-Plane for prime focus case

In order to explain the reason why the mesh0 gives a worse radiation pattern, the free node positions of the mesh0 in the $\vec{Z}$ direction were optimized base on the optimization strategy given in section 3 with the $\vec{X}$ and $\vec{Y}$ coordinates unvaried. With the optimal node positions obtained, a new mesh was obtained and denoted as mesh01. The axial deviation from best-fit paraboloid was calculated and the contours graph is shown in Fig.11 for both the mesh0 and mesh01. Also, there is a comparison of the radiation pattern for the mesh01 with the ones for the ideal surface and the mesh0 in Fig.12.

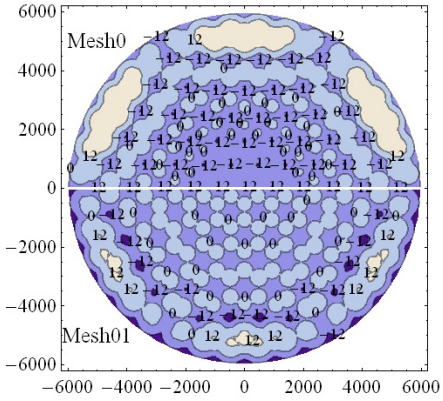

Fig.11 Axial deviation distribution for mesh0 and mesh01

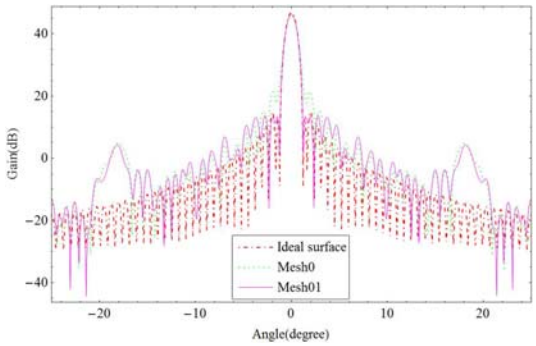

Fig.12 Far field patterns in E-Plane for mesh0 and mesh01

From Fig.11, it can be seen that the axial deviation distribution is improved by the node position optimization process since the mesh01 (see the lower half pie) has more uniform deviation distribution than the mesh0 (see the upper half pie) does. Fig.12 shows that the mesh01 has a better radiation pattern than the mesh0 does.

Now, it may be concluded that the introduction of node position optimization is significant for getting a better surface profile. It means that, with all net nodes exactly on a paraboloid may not be a good idea in designing a surface profile of mesh reflector under the uniform tension strategy.

Meanwhile, it can be seen from Figs. 9, 10 and 12 that only the main beams and nearby sidelobes are affected significantly by the improvements made in the mesh1 and mesh2. For this reason, a smaller range of angles is taken when the offset configuration cases are discussed in section 5.2.

5.2 Offset configuration

5.2.1 Calculation of the nets

In the offset case, a 6 by 10 diamatic net pattern is considered. The initial net pattern on the antenna aperture is shown in Fig. 13. All the initial nodes, including the fixed boundary nodes, were positioned exactly on the paraboloid surface given by Eq. (1).

For a 100N uniform tension in the net, all the form-finding approaches converged to stabilized equilibrium positions. In Fig.14, only the resulting mesh1, described in the local

coordinate system ($\vec{X}', \vec{Y}', \vec{Z}'$), is presented. Other details of the results are listed in Table 2 for a comparison. The faceting rms errors shown in Table 2 are all figured out by using Eq. (7).

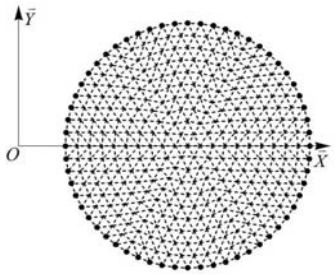

Fig.13 A 6 by 10 diamatic net pattern for the offset case

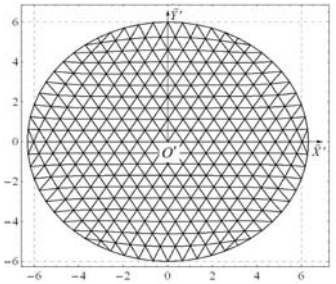

Fig.14 Offset configuration net under uniform tension

Table 2 Form-finding results for the offset configuration

	Mesh0	Mesh1	Mesh2
Iterations	48	50	50
Converged max$\left\|(T_j - T_u)/T_u\right\|$	1×10^{-6}	1×10^{-6}	1×10^{-6}
Converged max$\left\|\Delta\vec{X}_i'\right\|$ (mm)	0.0008	0.0009	0.0009
Faceting rms error(mm)	0.53	0.51	0.52
Parameter t (mm)	2.15	2.49	2.43
Average force in tension ties (N)	7.14	7.11	7.11
Standard deviation of forces in tension ties (N)	0.53	0.62	0.62

Table 2 shows similar results compared with Table 1. The uniform tension requirement is always well satisfied when the nodes converge to their stabilized equilibrium positions. However, because the reflector surface is finely meshed in this case, the differences among the faceting rms errors are smaller, so are the differences among the average forces in the tension ties.

It should be mentioned that, for the offset configuration case, the coordinates $X_i'^p$ and $Y_i'^p$ were slightly changed after the coordinate $Z_i'^p$ was found by the optimization process. It did have influence on the form-finding procedure, reflected in more iteration steps being taken for both the mesh1 and mesh2. But, since only two more steps were taken in this application, the influence was apparently small.

5.2.2 Radiation patterns

Here, it is also assumed that the RF reflective mesh will exactly follow the shape of the cable net, and there is no other but faceting error on the resulted mesh reflector, and the wave leakage throughout the mesh is ignorable. Moreover, the attachment of the nets to the antenna rim trusses implies that the boundary conditions are not necessarily compatible with the net patterns. The rim is realized with a 30-bay ring in the case of the AstroMesh [3] and the net is thus attached at 30 points to the ring truss, whereas it requires 60 points to fix a 6 by 10 diamatic pattern. For the cases like this, the method proposed in Ref. [4] can be used to generate new cables which can connect the main part of the cable net (resulted from the proposed form-finding approach) to the rim truss without changing the node positions and the cable tensions in the main part. Here, this specific method is not going to be discussed. The full net patterns of the resulting meshes were still used in the calculations for the far field radiation patterns.

The co-polar far-field radiation patterns, calculated at 20 GHz by the physical optics (PO) method in both the E-plane and the H-plane, are shown in Figs.15 and 16 respectively. Fig. 17 is the magnified image in the main beams of Fig. 15. In all these figures, the radiation patterns for the mesh1 and mesh2 are nearly coincident with each other. Compared to the radiation patterns of the mesh0, they are closer to the ones for the ideal surface. In the E-Plane, symmetry of the radiation pattern is kept only for the ideal surface, but when only the main beams are considered, it is the radiation pattern for the mesh0 which loses the symmetry because of a beam squint. The beam squint can be seen clearly in Fig. 17 and in Table 3 where the maximum directivities in the E-plane for the ideal reflector and for the mesh reflectors are listed.

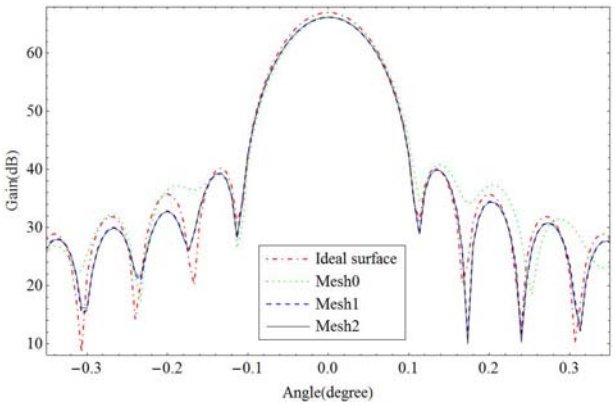

Fig.15 Far field patterns in E-Plane for offset configuration

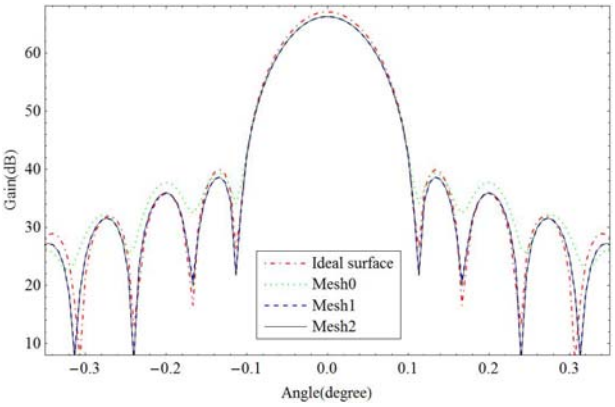

Fig.16 Far field patterns in H-Plane for offset configuration

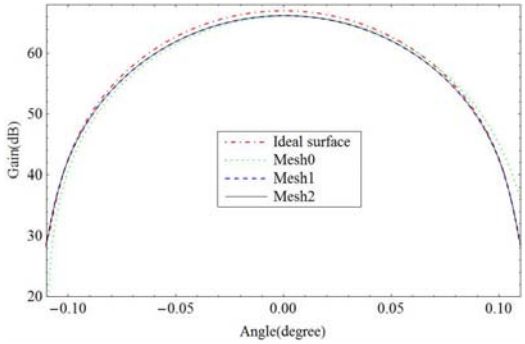

Fig.17 The magnified image of Fig. 15 in the main beams

Table 3 Maximum directivity in E-plane

	Ideal	Mesh0	Mesh1	Mesh2
Max directivity (dB)	67.04	66.18	66.23	66.23
Location (degree)	0	0.0028	0	0

These results suggest that even there is no much improvement to the reflector faceting rms error and in turn for the antenna gain in such a case, the mesh1 and mesh2 obtained by the proposed method provide better RF performance in comparison with the mesh0 obtained by the usual form finding method [4]. Note that the mesh1 and mesh2 really have much smaller faceting rms errors than the mesh0 in the prime focus case where the reflector is roughly meshed.

5.2.3 Further discussions

Based on the above results, it can be seen that there is no much space for reducing the reflector faceting rms error in this application without increasing the number of facets or the focal ratio. However, a much better result seemed to have been achieved in [9] for the same application investigated here. The result was a faceting rms error of 0.254mm compared to the one of 0.33mm given by Morterolle [4].

Two issues may be observed here. The first one is that both the faceting rms errors appeared in [4] and [9] were smaller than that listed in Table 2 (it is 0.53 mm for the mesh0). The second one is that a remarkable improvement was achieved in [9] but we think it shouldn't be that much. The key to answer these questions is the method used in calculating the faceting rms errors. In the method presented in [4], the faceting rms error of a mesh reflector was calculated by

$$\delta_{rms} = \left(\sum_{i=1}^{N} A_i (Z_i - Z_{g_i})^2 / \sum_{i=1}^{N} A_i\right)^{\frac{1}{2}} \quad (23)$$

where N represents the total number of facets in the mesh reflector; A_i is the projected area of triangular facet i on the plane of $(\vec{X},\vec{Y})$; Z_{g_i} is the position of the gravity center of triangular facet i on the vertical axis $\vec{Z}$ of the parent paraboloid and Z_i is the theoretical position of this point on the reference paraboloid surface calculated with the (X_{g_i}, Y_{g_i}) coordinates. The reference paraboloid, which minimizes δ_{rms}, is the best-fit paraboloid.

The equation for the best-fit paraboloid was

$$Z = (X^2 + Y^2)/(4F_{bf}) + t \quad (24)$$

where F_{bf} represents the focal length of the best-fit paraboloid and t represents the offset distance of the best-fit paraboloid in $\vec{Z}$ direction.

In order to compare our results with the ones given in [4] and [9], the faceting rms errors for the mesh1 and mesh2 were recalculated using their method (Eq. (23)) but without adjusting the focal length of the desired paraboloid ($F_{bf} = F$). The results are listed in Table 4.

Table 4 Faceting rms errors calculated by Eq. (23)

	Mesh1	Mesh2	Mesh3
Faceting rms error(mm)	0.18	0.17	0.13
Parameter t (mm)	3.21	3.16	3.25

Apparently, the faceting rms errors of both the mesh1 and mesh2 became smaller than the ones listed in Table 2. They are also smaller than the faceting rms errors listed in [4] and [9] for this case. The mesh2 now becomes the best reflector under this criterion compared with the mesh0, mesh1 and the one given in [9].

However, the mesh2 should not be the best result because Eq. (23) was not the objective function when it was figured out. By using Eq. (23) as the objective function to optimize the Z positions of the net nodes during the form finding procedure, one more cable net was obtained and denoted as mesh3. The faceting rms error for the mesh3 is also listed in Table 4. It is apparent that the mesh3 has an even smaller faceting rms error than the mesh2.

So far, it seems that the mesh3 should have the best RF performance for such an antenna. In order to verify this, the co-polar far field radiation patterns for the mesh3 in both the E-plane and the H-plane were figured out and shown in Figs. 18 and 19. Fig. 20 is the magnified image in the main beams of Fig. 18. Table 5 lists the maximum directivities in the E-plane for the ideal reflector and the mesh reflectors.

Table 5 Maximum directivity in E-plane (extended)

	Ideal	Mesh0	Mesh1	Mesh2	Mesh3
Max directivity (dB)	67.04	66.18	66.23	66.23	66.20
Location (degree)	0	0.0028	0	0	-0.0014

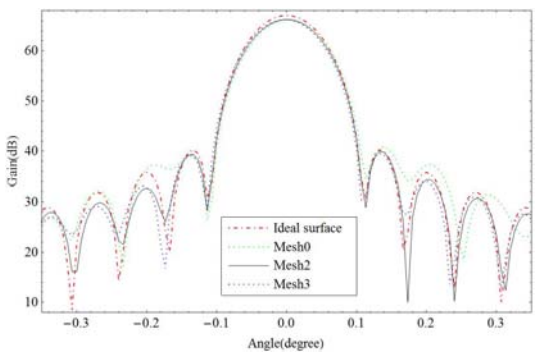

Fig.18 Far field patterns in E-Plane for the mesh3

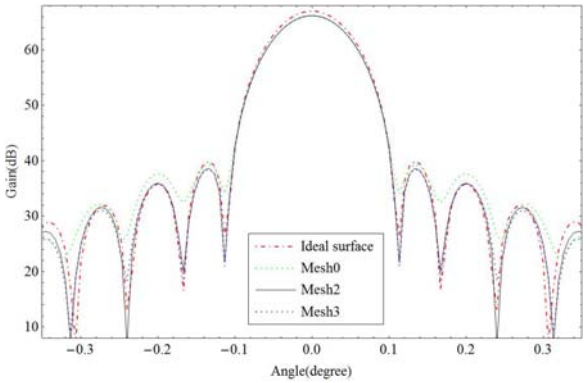

Fig.19 Far field patterns in H-Plane for the mesh3

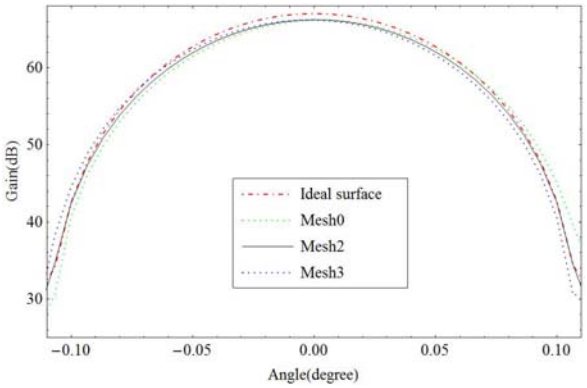

Fig.20 The magnified image of Fig. 18 in the main beams

It can be seen clearly in both these figures and Table 5 that the mesh3 does not have a better RF performance than the mesh2 even it has a smaller faceting rms error. The maximum directivity for the mesh3 is less than the one for the mesh2. Meanwhile, the radiation pattern for the mesh3 has a beam squint in the opposite direction in comparison with the one for the mesh0 in the E-plane.

In fact, the rms error calculated by Eq. (23) should not be applied into Eq. (4) for the predication of the effects of surface deviations on the radiation pattern and gain of an antenna because it is only an approximation of Eq. (22) and Eq. (22) is also an approximation of Eq. (7). To calculate the value of Eq. (22), integrations on triangular regions (Eq. (13)) are inevitable. Note that the integrant of Eq. (13) has a degree of 4 when $w(\vec{r})=1$, a quadrature rule of no less than order 4, which in turn means a quadrature rule of at least 6 integral points, should be used to get a fairly accurate result for Eq. (22). Since Eq. (23) only takes one integral point in calculating the integration of Eq. (13), much accuracy could be lost.

All of these show that a blindly seeking for minimizing of Eq. (23) does not make much sense to the performance improvement of a mesh reflector. However, it does not mean that the way in calculating rms error by Eq. (23) is meaningless. In fact, such estimation is often used by mechanical engineers in practice. To have a better understanding on such things, the faceting rms errors of mesh0 and mesh2 on a series of cases were calculated and listed in Table 6.

Table 6 Comparison of faceting rms errors for mesh0 and mesh2

Net pattern (6 by)	Ratio F/D_p	Mesh0		Mesh2	
		Our method (mm)	Previous method[4] (mm)	Our method (mm)	Previous method[4] (mm)
5	0.45	2.43	1.05	2.37	0.70
6	0.45	1.70	0.79	1.65	0.49
8	0.45	0.98	0.49	0.93	0.27
10	0.45	0.63	0.34	0.60	0.17
10	0.3	1.09	0.88	0.97	0.40
10	0.6	0.46	0.21	0.44	0.11

In these cases, both the aperture and the offset distance of the reflectors remain the same with the ones investigated above. Three different focal ratios and four different division numbers for the diamatic net patterns were considered. For the reason that when the focal ratio of the reflector changes the parameters of the illumination function should be changed accordingly, the results for mesh1, which should contain the chosen parameters for the illumination functions, are not listed here.

In Table 6, the faceting rms errors in the columns three and five are calculated by Eq. (22) and they are fairly accurate values for the real faceting rms errors. The ones in the columns four and six are calculated by Eq. (23) and are approximate values for the real faceting rms errors. It can be seen that, for both the mesh0 and mesh2, even there are quite obvious differences between the accurate values and the approximate values, the approximate values have the same trend with the accurate values. This means that the approximate rms errors calculated by Eq. (23) are suitable in most cases to give a rough estimation on some reflector designs, even if the estimation may not be taken rigorously for a final decision.

6. Conclusion

Based on the FDM, a new method to calculate a uniformly tensioned cable net is presented, where the faceting rms error is minimized to update the node positions in the iteration steps. Examples on both prime focus and offset configurations show the efficiency of the method proposed.

It may be concluded that the method proposed here is more effective than the one proposed in Ref. [4]. The results for the mesh2 are always close to the ones for the mesh1 and are better than the ones for the mesh0 in all the applications investigated. It is recommendable to use the axial faceting square error e_{zs} rather than the faceting square error e_s in a form-finding procedure to take the advantage of its simpler form.

REFERENCES

[1] Meguro, A., Harada, S., and Watanabe, M. Key technologies for high-accuracy large mesh antenna reflectors." Acta Astronaut, 2003,53(11): 899–908.

[2] A. H. Nayfeh and M. S. Hefzy, Geometric modeling and analysis of large latticed surfaces [R]. NASA CR-3156, 1979

[3] Thomson M W. The AstroMesh deployable reflector [C]. Antennas and Propagation Society, IEEE International Symposium，1999, 3: 1 516-1 519.

[4] Morterolle S, Maurin B, Quirant J, et al. Numerical form-finding of geotensoid tension truss for mesh reflector[J]. Acta Astronautica, 2012, 76: 154-163.

[5] TIBERT G. Deployment Tensegrity Structure for Space Applications [D]. Stockholm: Royal Institute of Technology Department of Mechanics，2002.
[6] Deng H, Li T, Wang Z. Design of geodesic cable net for space deployable mesh reflectors [J]. Acta Astronautica, 2016, 119: 13-21.
[7] Deng H, Li T, Wang Z, et al. Pretension Design of Space Mesh Reflector Antennas Based on Projection Principle [J]. Journal of Aerospace Engineering, 2014, 28(6): 04014142.
[8] Deng H, Li T, Wang Z. Pretension design for space deployable mesh reflectors under multi-uncertainty [J]. Acta Astronautica, 2015, 115: 270-276.
[9] H. Shi, B. Yang, H. Fang, “Offset-Feed Surface Mesh Generation for Design of Space Deployable Mesh Reflectors”, Proceedings of the 54th AIAA/ASME/ASCE/AHS/ASC Structures, Structural Dynamics, and Materials Conference, Boston, Apr. 17 - 11, 2013.
[10] H. Shi, B. Yang, M. Thomson, H. Fang, “Automatic Surface Mesh Generation for Design of Space Deployable Mesh Reflectors”, Proceedings of the 53rd AIAA/ASME/ASCE/AHS/ASC Structures, Structural Dynamics, and Materials Conference, Honolulu, HA, April 23 - 26, 2012.
[11] Li T, Jiang J, Deng H, et al. Form-finding methods for deployable mesh reflector antennas[J]. Chinese Journal of Aeronautics, 2013, 26(5): 1276-1282.
[12] Wang L, Dongxu L. Simple technique for form-finding and tension determining of cable-network antenna reflectors[J]. Journal of Spacecraft and Rockets, 2013, 50(2): 479-481.
[13] Ma X F, Song Y P, Li Z J, et al. Mesh reflector antennas: form-finding analysis review[C]//Proceedings of 54th AIAA/ASME/ASCE/AHS/ASC Structures, Structural Dynamics, and Materials Conference. Boston, Massachusetts: AIAA. 2013.
[14] Yang D, Zhang S, Li T, et al. Preliminary design of paraboloidal reflectors with flat facets[J]. Acta Astronautica, 2013, 89: 14-20.
[15] Ruze J. Antenna tolerance theory--a review[C]//IEEE Proceedings. 1966, 54: 633-642.
[16] Dunavant D A. High degree efficient symmetrical Gaussian quadrature rules for the triangle [J]. International journal for numerical methods in engineering, 1985, 21(6): 1129-1148.